Integrated Modeling of Equilibrium Reconstruction in Tokamaks

Ana Margarida Jorge dos Santos
ana.m.santos@tecnico.ulisboa.pt

Instituto Superior Técnico, Lisboa, Portugal

July 2021

Abstract
The Reconstruction of MHD equilibrium is fundamental to the understanding of fusion plasma physics. It is necessary for data diagnostic analysis, to the study of plasma stability, transport, confinement to the control of the plasma, among others. In this work the equilibrium of an ICRH and NBI heated JET discharge is studied. The equilibrium is reconstructed with progressively more information using the EQUAL code (in the EQSTABIL RECONSTRCUT workflow). Starting by using only magnetic diagnostics, then adding the thermal pressure calculated using the HRTS diagnostic's measurments, then the energetic particle pressure component determined numerically using the CYRANO and StixReDist codes (in the HCD workflow) and finally adding the polarimetry and interferometry diagnostics. The results were validated using the MHD spectroscopy, specifically the $(3, 2)$ NTM mode. This was done within the EUROfusion Integrated Modeling framework, WPCD. The energetic particle pressure components (of deuterium and hydrogen) were found to be located at the core of the plasma and to have maximum values similar to the thermal pressure values, so that the total pressure profile has a maximum (which is located at an off-axis position), around three times larger than the thermal pressure. Reconstruction using a discharge with such high energetic particle pressures proved to be a challenge. The reconstructed pressure doubled when compared with the thermal pressure and the maximum and minimum of the safety pressure and flux surface averaged toroidal current density were displaced to an off-axis position. The addition of the polarimetry and interferometry diagnostics improves the reconstruction, but only slightly.
Keywords: Tokamak, JET, equilibrium reconstruction, ICRH, energetic particle pressure.

1. Introduction

Over the past decades, abounding evidence for climate change and other environmental impacts of the currently available energy sources have surfaced. These, coupled with the increasing population, technology, and standard of living and thus, the increase in energy consumption, indicate the need for an alternative solution for the world's energy challenges. Nuclear fusion presents a viable and environmentally friendly source of energy production.

The most promising method to achieve nuclear fusion is through magnetic confinement, a reactor concept based on the so-called tokamak [1] and using the fusion reaction of Deuterium and Tritium in the plasma state. Tokamak is a toroidal asymmetric device that confines the plasma using magnetic fields. The external toroidal field coils create the toroidal magnetic field (B_ϕ). This field creates a drift in the outward direction. To prevent it, a poloidal field (B_θ) is created by a toroidal current. In the end, the magnetic field lines are helices, which rotate slowly in the toroidal direction.

In order to achieve high enough temperatures, external heating methods (besides the transformer effect) are required, such as the injection of neutral highly energetic particles into the plasma (NBI) or radio-frequency waves with frequencies similar to the ions and electron cyclotron frequencies (ICRH and ECRH). These create energetic particles (non-Maxwellian distribution in energy), which can have a significant impact on the total plasma pressure.

When enough external heating power is added to the plasma, a high confinement mode (H-mode) can be achieved. This mode is characterized by a steep gradient at the edge of the plasma pressure profile (a pedestal that shifts the entire pressure profile up).

For the purposes of this thesis, the diagnostics can be divided into magnetic, current, and kinetic diagnostics. Magnetic diagnostics (e.g., flux loops, poloidal field probes) measure the total plasma current and the magnetic fields and poloidal flux next to the plasma boundary. Current diagnostics (e.g., polarimetry which gives the Faraday rotation angle of a laser beam when crossing the plasma) give in-

formation on the internal magnetic field. Kinetic diagnostics (e.g., Thomson scattering, which measures the electron temperature and density, electron cyclotron emission, which measures the electron temperature, interferometry, which measures the integrated density) give information on the ion and electron temperatures and densities, and so allow the determination of the pressure.

Some of these diagnostics need equilibrium reconstruction to analyze of the data, while others are used by the reconstruction algorithm to obtain more information. The addition of the pressure profile obtained by some diagnostics and numerical codes is known to alter the reconstructions significantly, increasing their accuracy.

The equilibrium reconstruction is also necessary to the study of the plasma stability (and so it is important in preventing plasma instabilities), to the study of transport, confinement, efficiency, to control the plasma, among others.

The objective of this work was to reconstruct the MHD equilibrium for a plasma discharge of the JET Tokamak[2] heated with ICRH and NBI, using the EQUAL equilibrium reconstruction code [3] with increasing levels of information on the plasma state either from diagnostics or numerical codes. First, only using magnetic diagnostics, then proceeding to add the thermal pressure (calculated using the Thomson scattering diagnostics, HRTS), then adding the pressure from energetic particles calculated from numerical codes that simulate the effects of external heating on the plasma, and then adding the information for the interferometry and polarimetry diagnostics. This is done within the WPCD framework. The results of these reconstructions were validated using MHD spectroscopy.

2. Background

In this section, a small introduction to MHD Equilibrium and Equilibrium codes will be made.

2.1. Equilibrium

In order to maintain the magnetic confinement, the whole plasma must be kept under force equilibrium, i.e., the outward expansion force due to the plasma pressure must be balanced by the opposing magnetic forces. In order to study the equilibrium, a single-fluid plasma model known as MHD is used ($\mathbf{J} \times \mathbf{B} = \nabla p$, $\nabla.\mathbf{B} = 0$ and $\nabla \times \mathbf{B} = \mu\mathbf{J}$), where p is the plasma pressure, $\mathbf{B}$ is the magnetic field, $\mathbf{J}$ is the current density and μ is the magnetic permeability. These assume that the plasma is in a steady state ($\frac{\partial}{\partial t} = 0$) and static ($\mathbf{v} = 0$).

These equations imply the existence of so-called magnetic flux surfaces with characteristic properties: closed nested toroidal surfaces where the magnetic and current density lines lie and where the pressure and poloidal magnetic flux ψ are constant.

Using MHD equations, the Grad-Shafranov Equation (Eq.1) can be derived [4]. It can be extended to vacuum, external conductors, and ferromagnetic materials. In this equation, the (R, ϕ, Z) cylindrical coordinates are used, F is such that $F = B_\phi R$, J_ϕ is the toroidal current density, and $\Delta^*\psi$ is described as in Eq.2.

$$\Delta^*\psi = -\mu_0 R^2 \frac{dp}{d\psi} - F\frac{dF}{d\psi} = -\mu_0 R J_\phi \qquad (1)$$

$$\Delta^*\psi = \frac{\partial^2\psi}{\partial Z^2} + R\frac{\partial}{\partial R}\left(\frac{1}{R}\frac{\partial\psi}{\partial R}\right) \qquad (2)$$

2.2. Equilibrium codes

There are many types of equilibrium codes. In this work, a direct, free-boundary reconstruction code is used. These reconstruction codes aim to determine the topology or distribution of the magnetic field of the magnetic flux surfaces as well as the pressure, toroidal density current, and F function and safety factor profiles.

This is done by alternating between two steps: (1) solving Eq.1 numerically assuming that the pressure derivative and FF' function profiles can be represented as a linear combination of basic functions (y_n) which can be polynomials, tension splines, etc. So that $p' = \sum_n \alpha_n y_n$ and $FF' = \sum_n \gamma_n y_n$, where α_n and γ_n are unknown parameters, and (2) minimizing the squared error function ($\chi^2 = \sum(Measurement_i - Result_i/uncertainty_i)^2$) between the results (simulated measurements) and the diagnostic measurements weighted by the measurements' uncertainties to get new α_n and γ_n coefficients.

The measurements used in the reconstruction can be: (1) only magnetic, and so, the reconstruction algorithm uses the plasma current, poloidal flux, and the external magnetic field as constraints.

(2) Magnetic and from current diagnostics, adding constraints to the internal magnetic field, flux surfaces, and current density and thus, allowing for a better reconstructed safety factor and current density profiles as well as magnetic surface distribution.

(3) Magnetic and from the kinetic diagnostics, adding a constraint to the pressure profile. This allows for a better reconstructed pressure profile, especially on the pedestal region. Numerical codes can be used to calculate the distribution of energetic particles (non-Maxwellian) and so to calculate the total pressure profile.

The pressure profile is calculated by $P(\psi) = (n_i + n_z)T_i + n_e T_e + P_{fast}$, where n_i, n_z and n_e are the ion, impurity, and electron densities respectively, T_i and T_e and the ion and electron temperatures and P_{fast} is pressure from energetic particles.

T_e, T_i, n_e and come from measurements and n_i and n_z from the quasi-neutrality condition. These measurements usually come from in function of (R, Z), so they must be mapped into the same poloidal flux surfaces (that come from an initial magnetic only reconstruction). In this work, some simplifications are made so that the pressure is calculated by $P_{th}(\psi) = 2n_eT_e$, both measurements coming from the HRTS diagnostic.

3. Setup

3.1. Data

In this work, the #90198 shot of JET [2] is used.

Fig.1, provides some information about this shot. It can be seen that both NBI and ICRH are used. The NBI heating is used in the $t = [45.4; 49.8]s$ interval with $\sim 8.9MW$ of power at its maximum. The ICRH is used in the $t = [46.5; 50.5]s$ interval with $\sim 6.0MW$ of power at its maximum. It can also be seen that the sawtooth instability, associated with the presence of $q = 1$ magnetic surface, only appears at $t \sim 50.5s$ (see the regular spikes in the central channels of the ECE diagnostic). Since this shot has both NBI and high power ICRH, which lead to a significant energetic ion content, it can be quite challenging to model. Fig.2, presents the

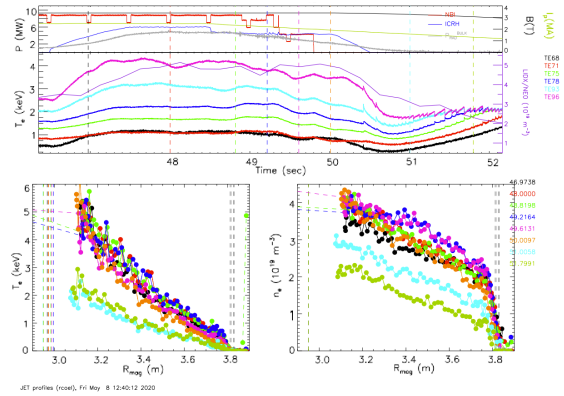

Figure 1: On the top: time evolution of NBI power (in red) and ICRH power (in blue), of the plasma current (in green) the magnetic field (in black), and the radiated power (in gray). In the middle: the electron temperature measured with different ECE channels is presented. In the bottom: the electron temperature and density measurements with HRTS in function of R_{mag} (the major radius along the horizontal plane containing the magnetic axis) for several time slices. Shot=90198.

toroidal mode spectra from the dominant MHD activity. A stronger line at $f \sim 12kHz$, corresponding to the toroidal mode number of $n = 2$, can be seen at $t = [47.0; 50.0]s$, the poloidal mode number is found to be $m = 3$. This mode is believed to be an $(n = 2, m = 3)$ Neoclassical Tearing Mode and it is resonant in the magnetic surface characterized by $q = 1.5$. The position of this surface will be used in the validation of the equilibrium reconstruction.

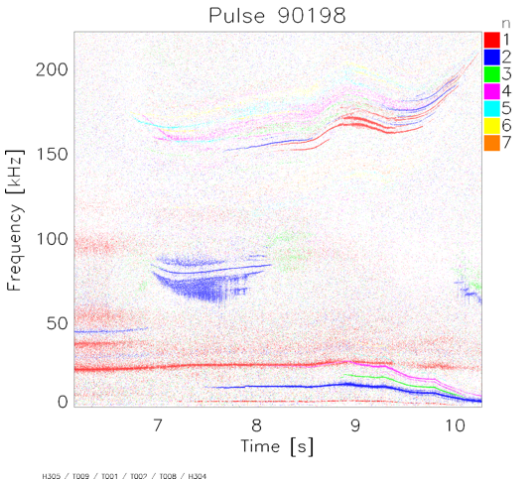

Figure 2: Time evolution of the toroidal mode spectra for the dominant MHD activity observed in shot 90198. The frequencies $f \sim [150 - 200]kHz$ correspond to Toroidal Alfvén Eigenmodes (TAEs), the $n = 2$ at $f \sim 12kHz$ is a $(3, 2)$ Neoclassical Tearing Mode (NTM) resonant at the $q = 3/2$ magnetic surface. The $n = 2$ mode at $f \sim 80kHz$ is believed to be a High Order Geodesic Acoustic Eigenmode (HOGAE) [5]

3.2. Codes and Workflows

The equilibrium reconstruction code used is EQUAL [3]. This code is based on EFIT [6] and is developed within the European Task Force on Integrated Tokamak Modelling (ITM-TF) [7]. This code is inserted in both the EQSTABIL RECONSTRUCT AND REFINE, and the EQSTABIL RECONSTRUCT AND REFINE Time Loop workflows. These were used in this work to make some of the equilibrium reconstructions either for one time slice ($t = 48.0s$) or for multiple time slices.

To simulate the ICRH for a single time, the heating and current drive workflow is used. This workflow used the CYRANO [8] code to simulate the launching, propagation, and absorption of the radio-frequency waves through the plasma (by solving Maxwell's equations) in order to give an initial particle distribution and the StixReDist [9] Fokker-Plank code, which solves the equation with the same name in order to give the time evolution of the initial distribution.

4. Methods

4.1. Validation of the results

The reconstruction code has various parameters that can be changed to get a better or worse equilibrium reconstruction. Most important for this work

are the weights and placement of the B-spline knots and the pressure profile weights.

The EQUAL code minimizes the cost function, as seen in section 2, and so it chooses an equilibrium reconstruction depending on the measurement errors.

In order to choose the best parameters for the reconstruction, various metrics are used: (1) the magnetic errors, (2) the shape of the pressure profile (if it stays positive close to the boundary or how similar it is to the given pressure profile) (3) the safety factor and flux surface averaged toroidal current density profiles shape (expected to be the ones characteristic of H-mode) (4) The existence or not of the $q = 1.0$ magnetic surface and thus the sawtooth instability (5) Safety factor value in the position of the $(3, 2)$ mode according to the ECE and magnetic diagnostics.

To compare the safety factor values (as required in step (5)): Look for the ECE channels that correspond to π jumps (a signature of magnetic reconnect characteristic of NTMs) in the cross power spectral density between the temperature fluctuation and magnetic signals, then get the (R, Z_{ECE}) position of the channel from the corresponding cyclotron resonance and get the q value from the equilibrium reconstruction in that position and compare to the expected value of $q = 1.5$.

4.2. Modeling strategy and sensitivity analysis

Seven reconstructions were made using progressively more information: using only the magnetic diagnostics, then adding the thermal pressure profile, then the total pressure profile, and then the Faraday rotation angle and integrated density from the polarimetry and interferometry diagnostics to each of those. The seventh was to use a second iteration of the total pressure.

Then the sensitivity of the heating and current drive workflow to using kinetic reconstructions with different thermal pressure profiles was also studied.

These reconstructions were made first for the $t = 48.0s$ time slice. As can be seen in Fig.1, in this time slice, both ICRH and NBI are being used. During the tests, it was found that in this time slice, the pedestal characteristic of the H-mode was well defined and that the stored energy was at its maximum. Then they were repeated for the time interval $t = [46.0, 52.0]s$ with $\Delta t = 0.1s$.

The methods to get each of these reconstructions are presented next.

4.2.1 Magnetic only Reconstruction

The workflows mentioned in section 3 are used to make a magnetic reconstruction that uses only the magnetic measurements from the differential and flux loops, from the pick-up and poloidal field coils and iron magnetization along with the plasma current and the diamagnetic signal, for both the $48.0s$ and from $46.0s$ to $52.0s$ with a time step of $0.1s$.

4.2.2 Kinetic Reconstruction using the thermal pressure

The same workflow was then used to make an equilibrium reconstruction using the magnetic measurements and the thermal pressure profile using the following steps: (1) Make an equilibrium reconstruction using only the magnetic diagnostics using the EQUAL code to get $\psi(R, Z)$ function. (2) Map the electron temperature and density from the HRTS diagnostic into the flux surfaces from the first reconstruction, i.e., transform $T_e(R, Z)$ into $T_e(\psi)$. (3) Calculate the thermal pressure by $P_{th}(\psi) = 2T_e n_e$ (the ion temperature and density are assumed to be the same as the electron ones). (4) The new reconstruction is made with the thermal pressure profile as a constraint along with the magnetic diagnostics for both the $48.0s$ and from $46.0s$ to $52.0s$ with a time step of $0.1s$.

4.2.3 Kinetic Reconstruction using the total pressure

During the tests made, it was found that the energetic particle component of the pressure from ICRH was far bigger than from NBI, so only the ICRH was used in the calculation of the total pressure. In order to do this reconstruction, the following steps were followed: (1) a kinetic reconstruction using the thermal pressure profile was made using the EQSTABIL RECONSTRUCT AND REFINE. (2) The HRTS diagnostics are mapped into that reconstruction's flux surfaces and used to calculate a new thermal pressure. (3) The Heating and Current drive workflow is used to calculate the energetic particle pressure component due to the ICRH heating by first updating the reconstruction with the CHEASE code, then the launching, propagation, and absorption of the waves are simulated with the CYRANO code, then the StixReDist code is used to evolve the distribution function in time, finally, the energetic particle pressure is calculated. (4) The total pressure profile is calculated using $P_{tot} = P_{thermal} + P_{fast}$ (the thermal pressure is the one from point 2 and there is some extrapolation of the data in the core region of the profile) (5) The final reconstruction is made using the total pressure profile as a constraint for $46.7s$, $46.9s$, $47.1s$, $47.5s$, $48.0s$, and $49.0s$ time slices.

4.2.4 Effect of the kinetic reconstruction on the total pressure profile

Since the heating and current drive codes use both the equilibrium and coreprof CPOs as input and

that the ICRH deposition, when located in the deep plasma core, is quite sensitive to the equilibrium flux map, we can anticipate that there will be different total pressure profiles for different equilibrium reconstructions. Thus, in this section, various total pressure profiles were made using different equilibrium reconstructions.

In order to do it, a magnetic equilibrium reconstruction was made using the EQUAL code, then the diagnostic data from Thomson scattering was mapped and the thermal pressure profile calculated. Using this thermal pressure profile, different equilibrium reconstructions were made using EQUAL with different pressure weights (using different portions of the pressure profile).

4.2.5 Kinetic Reconstruction with two iterations for the calculation of the total pressure

Given that in the previous section, it was found that the total pressure depends heavily on the equilibrium reconstruction, it was hypothesized that adding another iteration to the reconstruction could improve the results. In order to test this hypothesis, the following steps were followed. (1) Making a kinetic reconstruction using the total pressure profile. (2) calculating the thermal pressure using this equilibrium. (3) Using the Heating and current drive workflow, a second version of the total pressure was calculated (4) Fourth equilibrium reconstruction using the new total pressure profile. This was done for the $48.0s$ time slice.

4.2.6 Kinetic Reconstruction using the total pressure, interferometry, and polarimetry diagnostics for $t = 48.0s$

When looking at the results of the previous section, it was concluded that when using the total pressure as a constraint it is very difficult to get an agreement between the reconstructed and total pressure profiles and that the safety factor and flux surface averaged toroidal current density profiles become hollow. This is thought to be due to the fact that, in the core only the pressure profile has constraints and the FF' is free to change. So the Faraday rotation angle and integrated density from lines of sight that pass close to the magnetic axis are added to the reconstruction (channels 3,5 and 7 of the interferometry and polarimetry diagnostics).

These were added to the first three reconstructions described above.

5. Results

5.1. $t = 48.0s$

As stated in the methods section, seven different equilibrium reconstructions were made using progressively more data.

First, the magnetic reconstruction was made (equil 1), then the thermal pressure profile was determined, and then the kinetic reconstruction using the thermal profile was made (equil 2). From the first two reconstructions, it can be seen that the addition of the thermal pressure constraint to the reconstruction, results in the appearance of the pedestal at $\rho_{pol,norm} = 0.97$ in the pressure profile along with the equivalent structure in the flux surface averaged toroidal current density profile, as can be seen in Fig.3 and 4. These are a characteristic of the H-mode plasma and are not present in the magnetic only reconstruction. Between these two reconstructions (magnetic and thermal profile) we can also see a decrease in the core pressure (from $109kPa$ to $76kPa$) and a decrease in the core flux surface averaged toroidal current density (from $1870kAm^{-2}$ to $1600kAm^{-2}$). It can also be seen that the values of the magnetic sensor errors become larger and that the MHD marker errors become better (from values around 12% to values around 4%), see Tab.5.1.

Then the component pressure profile due to ICRH energetic particles was determined. It was found that the energetic deuterium pressure is concentrated at $\rho_{pol,norm} < 0.25$ and has a maximum of $107kPa$ and that the energetic hydrogen pressure is concentrated at $\rho_{pol,norm} < 0.4$ with a maximum of $65kPa$. When the energetic particle components of the pressure are added to the thermal pressure profile to get the total pressure (total 2), the maximum of the profile increases from $70kPa$ to $220kPa$ (it more than triples) and is shifted from the magnetic axis to $\rho_{pol,norm} = 0.12$. The value at the axis goes from $P_{th}(0) = 70kPa$ to $P_{tot}(0) = 160kPa$ (it approximately doubles).

The following reconstruction, was the one that uses this total pressure profile as a constraint along with the magnetic diagnostics (equil 3). Reconstructing the equilibrium with this pressure profile was found to be difficult. The resulting pressure profile does not have a similar shape to the one used as a constraint (Fig.3) at the core (the pedestal fit is still good). In fact, in all the tests made, the pressure profile was always monotonic. That being said, the safety factor and flux surface averaged toroidal current density profiles become non-monotonic (with their minimum and maximum off-axis), which are not the expected shapes for these profiles.

When comparing to the previous reconstruction (the one with the thermal profile as a constraint), it can be seen that the pressure at the core doubles, the maximum of the flux surface averaged toroidal current density profile is shifted to an off-axis position and increases to $2240kAm^{-2}$ (at $\rho_{pol,norm} \sim 0.29$), though the axis value decreases

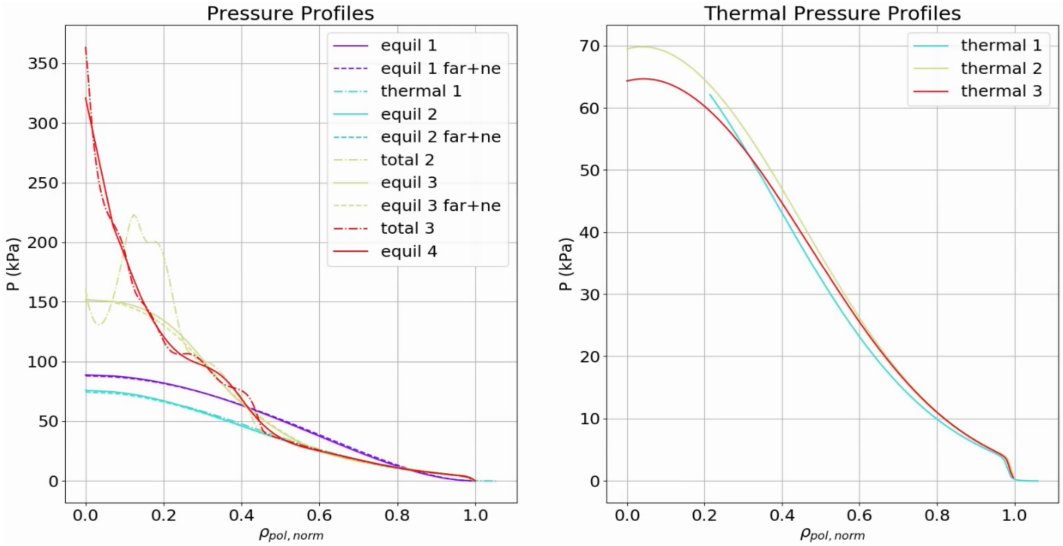

Figure 3: On the left: Reconstructed pressure profiles and the pressure profiles used as constraints in the reconstruction. On the right: Thermal pressure profiles determined using the HRTS diagnostic and the first three reconstructions. Time=48.0s

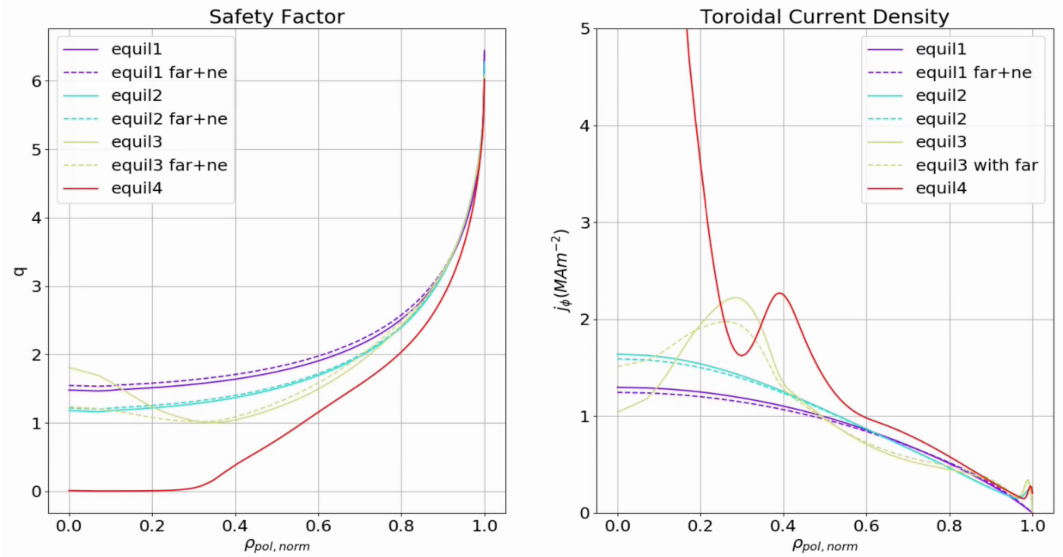

Figure 4: On the left: reconstructed safety factor profiles. On the left: reconstructed flux surface averaged toroidal current density profiles. Time=48.0s

$B_\phi(T)$	equil1	equil1+far+ne	equil2	equil2+far+ne	equil3	equil3+far+ne	equil4
3.044	12.3	16.8	0.4	2.2	24.7	16.8	14.3
3.079	9.4	13.8	4.0	2.1	30.8	24.1	22.8
3.919	12.7	17.3	5.8	3.8	18.0	12.5	18.1
3.937	13.7	18.2	4.6	2.7	15.9	10.4	15.7

Table 1: EQUAL safety factor error value that corresponds to the $n = 2$ and $m = 3$ mode when compared to $q = 1.5$.

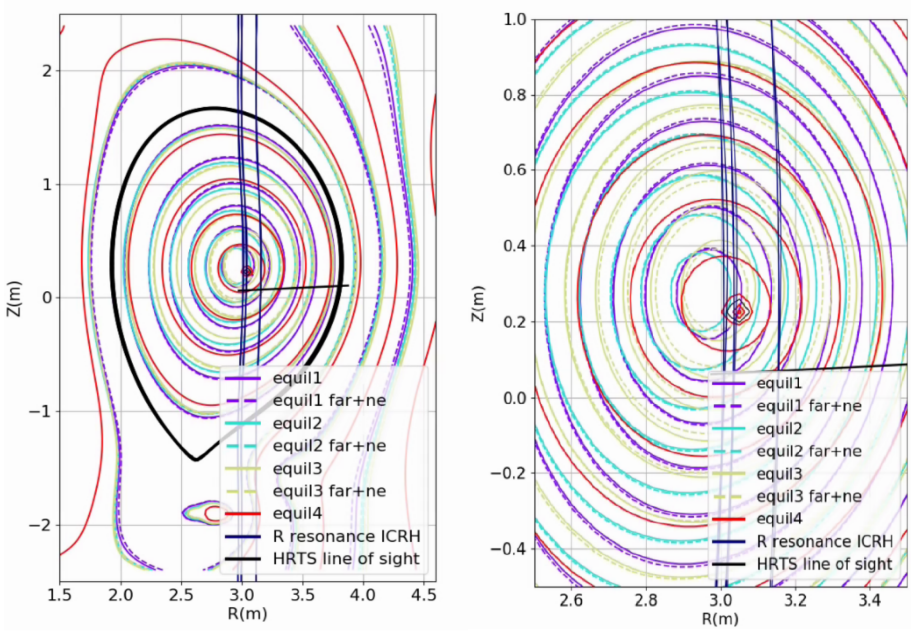

Figure 5: Contour plot of the flux surfaces for the seven reconstructions. On the right is a zoom to the area around the magnetic axis.

to $1050kAm^{-2}$, the safety factor profile changes as well, its minimum is shifted to $\rho_{pol,norm} \sim 0.35$ (see Fig.4). The addition of the total pressure also results in a shift of the flux surfaces to the right (see Fig. 5). On average the magnetic sensor errors improve, and the MHD marker errors worsen.

Then this equilibrium was used to calculate a new thermal pressure, energetic particle component of the pressure and so a new total pressure profile (total3). This new total profile can be seen in Fig.3, this profile is closer to being a decreasing function and has its maximum on the magnetic axis.

The value is much higher, at $\sim 350kPa$. This profile was used to make another reconstruction (equil 4). It results in a pressure profile that matches the constraint better, with a maximum of $\sim 325kPa$ (see Fig.3). However, in spite of the maximum and minimum of the flux surface averaged toroidal current density and safety factor profiles returning to the magnetic axis their values are not right (see Fig.4), too high and too close to zero respectively. The magnetic errors worsen and some of the MHD marker improve (Tab.5.1).

On the right of Fig.3, the thermal pressures calculated using different equilibriums can be seen. We can see that for the same value of pressure (same electron density and temperature, same data point, same R and Z), from the first to the second mapping, the values are shifted to the right (bigger $\rho_{pol,norm}$) and from the second to the third, there is a shift to the left (to a smaller value of $\rho_{pol,norm}$). These shifts can be explained either by fitting errors or by the geometry, different positions of the flux surfaces in each equilibrium used by the mapping.

By looking at Fig 5, it can be seen that the positions of the flux surfaces do change in each iteration, getting more similar as they reach the boundary (which also happens in the thermal profiles), their differences are mostly on the core region. From the first to the second equilibrium the surfaces shift to the left and from the second to the third they shift to the right. So (from the second to the third equilibrium) the same point in (R,Z), the same value of pressure, corresponds to a surface closer to the axis, so a smaller value of $\rho_{pol,norm}$, and so there is a shift of that point to the right. The shifts are due to the geometry.

Since the ICRH deposition position (in R, Z) does not change and since using bigger pressure profiles on the reconstruction results in a bigger Shafranov shift (magnetic axis moves to the right), the magnetic axis would get progressively closer to the deposition position leading to spikier pressure profiles (more iterations would not help in getting a good reconstruction).

The next step was to add the Faraday rotation angle and the integrated density to the first three reconstructions. The one with the magnetic diagnostics, the one with the thermal pressure profile, and the one with the total pressure profile (equil1+far+ne, equil2+far+ne and equil3+far+ne respectively). The main differences caused by this addition are in the core of the profiles, accompanied

by differences in the position of the flux surfaces. For the thermal pressure reconstruction, there is an improvement in the MHD marker errors. For the total pressure reconstruction, there is also an improvement in the MHD marker errors some improvement on the magnetic sensor errors, a small improvement of the curvatures of the safety factor and toroidal density current, and the flux surfaces are shifted to the right.

A final test was made to see how different kinetic equilibrium (with thermal pressure) affect the total pressure profile. In Fig.6 the results are presented. It can be seen that the maximum values and their position change, the profiles' shapes can be different, but in all the tests, the deposition of the energy is off the magnetic axis. The majority of the differences come from the energetic deuterium pressure and the thermal pressure profiles.

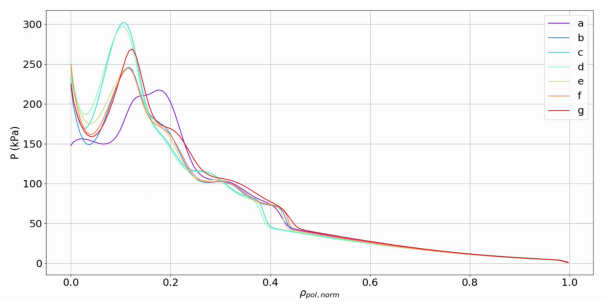

Figure 6: Total pressure profiles made with different kinetic equilibriums. 'a' was made with an equilibrium that uses the whole of the thermal pressure profile, 'b' with the values of the pressure profile at $\rho_{pol,norm} > 0.75$, 'c' for $\rho_{pol,norm} > 0.80$, 'd' for $\rho_{pol,norm} > 0.90$, 'e' for $\rho_{pol,norm} > 0.95$, 'f' for $\rho_{pol,norm} > 0.97$ and 'g' not using the thermal profile.

5.2. Timeloop

In this section, the same reconstructions were made but for several time slices. Beginning with the magnetic only reconstruction, then as before, with the mapping of the HRTS diagnostics and calculation of the thermal pressure profile followed by the kinetic reconstruction using the thermal pressure profile.

In Fig. 7, 8, and 9 the magnetic reconstruction pressure profile, the mapped thermal pressure profile, and the kinetic reconstruction pressure profile are plotted as a function of time.

As can be seen, in the first figure, we can see that the pedestal is not visible in the second figure we can see that the pedestal is formed at $46.7s$ (which matches the ICRH start time) and disappears at $49.7s$ (NBI and ICRH power start to decrease). The increase in the core pressure (at $\rho_{pol,norm} < 0.2$) starts at around $47.0s$ and reaches a maximum at

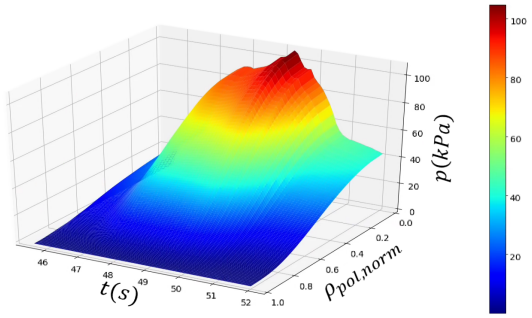

Figure 7: Pressure profile obtained from the equilibrium reconstruction using only the magnetic diagnostics in function of time and $\rho_{pol,norm}$

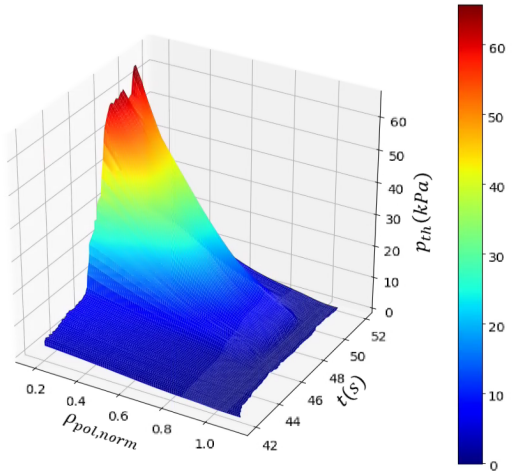

Figure 8: Thermal pressure calculated with the electron density and temperature from Thomson scattering in function of time and $\rho_{pol,norm}$

around $48.0s$ which can also see seen in the third figure. There is a dip in the core pressure at around $50.0s$ followed by an increase at around $51.0s$, which can also be seen in the third figure, and the values of safety factor, pressure in the magnetic axis (Fig.10 and 12) but not on the stored energy (Fig.11). This hints that the decrease in core pressure is accompanied by an increase in the pressure outside of the core and the second increase in the core by a decrease in the rest of the pressure, which can be confirmed by the plot of the pressure profiles.

The Faraday rotation angle and integrated density are then added to these reconstructions. As can be seen, the biggest differences are seen in the flux surface averaged toroidal current density and safety factor values at the core, as expected since they add constraints to the FF' function, which decrease and increase respectively. The core pressure values do not change much, and the stored energy increases slightly when these diagnostics are added to the magnetic reconstruction but not when added to the kinetic reconstruction.

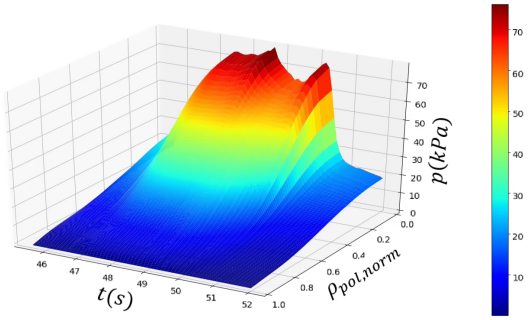

Figure 9: Pressure profile obtained from the equilibrium reconstruction using the magnetic diagnostics and thermal pressure in function of time and $\rho_{pol,norm}$

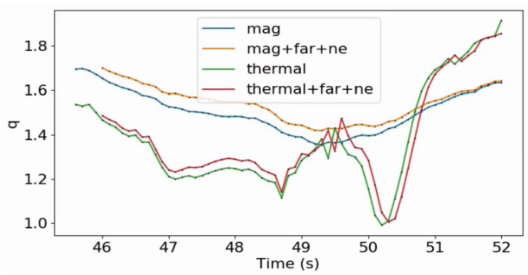

Figure 10: Safety factor at $\rho_{pol,norm} = 0$ in function of time.

Lastly, the total pressure profiles were calculated for various time slices and then these profiles were used to make the kinetic reconstruction.

When comparing the energetic deuterium pressure, it can be seen (in Fig. 13) that the maximums are in the same location $\rho_{pol,norm} = 0.12$ and that those values increase from $40kPa$ (at $46.7s$) to $152kPa$ at $47.1s$ and then decreases until $49.0s$ with $92kPa$, they do not follow the same behavior as the thermal pressure. The energetic deuterium pressure spreads to higher $\rho_{pol,norm}$ for $t > 47.5s$. When comparing the energetic hydrogen pressure, we can see that the pressure increases until $48.0s$ and only then starts to decrease. In Fig.13, the total pressure profiles are presented. It can be seen that for the other time slices the maximum pressure values are still off-axis at around $\rho_{pol,norm} = 0.12$, and that this value increases significantly from $46.7s$ to $47.1s$, while the ICRH power is increasing. In the $47.5s$ and $48.0s$, there is no increase in the maximum pressure but the curve widens. The maximum value decreases at the $49.0s$ as expected since the ICRH power also decreases.

The results of the reconstructions are also shown in Fig.13. We can see that the reconstructed pressure profiles never follow the shape of the total pressure profiles exactly (as with the $48.0s$ time slice, the reconstructed profiles are decreasing functions).

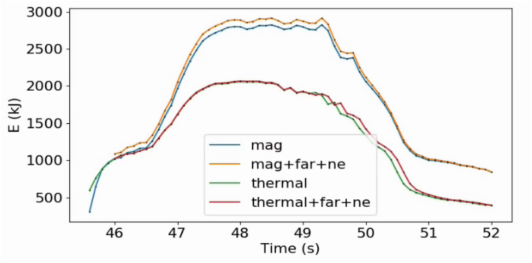

Figure 11: Stored energy $w_{mhd} = \frac{3}{2}\int pdV$ in function of time.

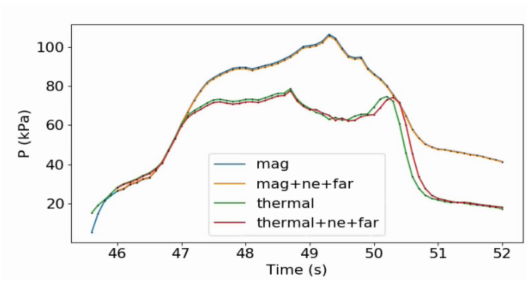

Figure 12: Pressure at $\rho_{pol,norm} = 0$ in function of time.

However, the maximum values of the two have the same behavior in time (they increase from $46.7s$ to $47.5s$ and then decrease). We can also see that the safety factor profile is monotonic for the $46.7s$, $46.9s$, and $49.0s$ time slices (where the total pressure is smaller) but it is for the other time slices. The flux surface averaged toroidal current density profiles either have an off-axis maximum (for the $47.1s$, $47.5s$, $48.0s$, and $49.0s$ time slices) or a step-like increase for $0 < \rho_{pol,norm} < 0.4$.

6. Conclusions

In this work, several equilibrium reconstructions were made with increasing levels of information for an NBI and ICRH heated JET discharge. It was found that the addition of the thermal profile as a constraint leads to reconstructions with better profiles and MHD marker error values, but worse magnetic sensor errors. It was found that the total pressure profile is 3 times larger than the thermal pressure profile (at the maximum values) and when using it as a constraint, a good reconstruction according to the validation metrics used becomes difficult (MHD marker error become worse, the pressure, safety factor, and flux surface averaged toroidal current density profile shapes are unconventional). The addition of polarimetry and interferometry diagnostics improves the reconstruction. The total pressure profile obtained does not seem to agree with the assumptions made in the equilibrium reconstruction.

In future work, a more accurate analysis of the

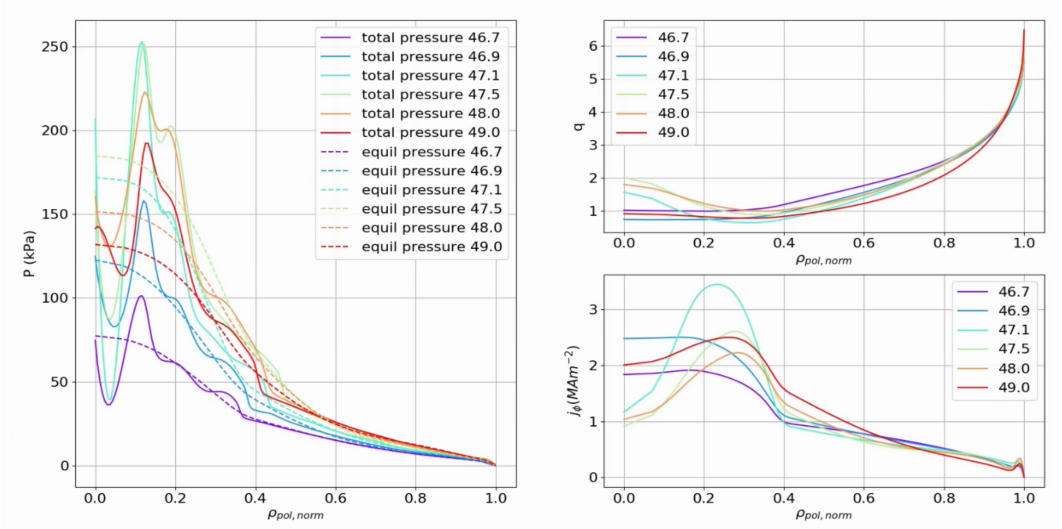

Figure 13: On the left: Reconstructed and total pressure profiles. On the top right: reconstructed safety factor profiles. On the bottom right: reconstructed flux surface averaged toroidal current density profiles.

heating should be made, one that takes into account the time evolution of the profiles including not only the heating but also the redistribution (diffusion and convection) and energy losses, consistent with various time scales of plasma transport. To some extent, this could entail interfacing the EQRECONSTRCUT and ETS (European Transport Simulator) [10] workflow.

Adding more magnetic sensors would increase the accuracy of the magnetic reconstruction so the mapping of the diagnostics would improve. Adding information about the ion temperatures and the different ions and electron densities to the calculation of the thermal pressure would make the thermal pressure more accurate.

Another addition to the analysis would be using the TAE (Toroidal Alfvén Eigenmodes) for validation along with the NTM and sawtooth crashes.

References

[1] John Wesson and David J Campbell. *Tokamaks*, volume 149. Oxford university press, 2011.

[2] JET - EUROfusion. https://www.eurofusion.org/devices/jet/. (Accessed on 10/15/2020).

[3] Wolfgang Zwingmann. Equilibrium analysis of steady state tokamak discharges. *Nuclear fusion*, 43(9):842, 2003.

[4] J Havlicek and J Urban. A magnetic equilibrium reconstruction in tokamak. *WDS'07 Proceedings of Contributed Papers Part II—Physics of Plasmas and Ionized Media*, pages 234–239, 2007.

[5] Paulo Rodrigues and Francesca Cella. High-order geodesic coupling of shear-alfven and acoustic continua in tokamaks. *arXiv preprint arXiv:2008.12753*, 2020.

[6] LL Lao, HE St John, Q Peng, JR Ferron, EJ Strait, TS Taylor, WH Meyer, C Zhang, and KI You. MHD equilibrium reconstruction in the DIII-D tokamak. *Fusion science and technology*, 48(2):968–977, 2005.

[7] Introduction to the EUROfusion project code development for integrated modelling — EUROfusion integrated modelling workflows 3.0 documentation. https://wpcd-workflows.github.io/introduction.html. (Accessed on 01/02/2020).

[8] P.U. Lamalle. *Nonlocal theoretical generalisation and tridimensional numerical study of the coupling of an ICRH antenna to a tokamak plasma*. PhD thesis, Université de Mons, LPP-ERM/KMS Report nr. 101., 1994.

[9] Dirk Van Eester and Ernesto Lerche. Simple 1d fokker–planck modelling of ion cyclotron resonance frequency heating at arbitrary cyclotron harmonics accounting for coulomb relaxation on non-maxwellian populations. *Plasma Physics and Controlled Fusion*, 53(9):092001, 2011.

[10] European transport simulator (ets) — eurofusion integrated modelling workflows 3.0 documentation. https://wpcd-workflows.github.io/ets.html. (Accessed on 06/07/2021).